Geophysical Research Letters

RESEARCH LETTER
10.1029/2018GL080868

A Geodesy- and Seismicity-Based Local Earthquake Likelihood Model for Central Los Angeles

Chris Rollins[1,2] and **Jean-Philippe Avouac**[1]

[1]Division of Geological and Planetary Sciences, California Institute of Technology, Pasadena, CA, USA, [2]Now at Department of Earth and Environmental Sciences, Michigan State University, East Lansing, MI, USA

Key Points:
- We develop a method to probabilistically estimate long-term earthquake likelihoods using a strain buildup model and a seismic catalog
- We infer that the maximum-magnitude earthquake in central Los Angeles is $M_w = 6.8 + 1.05/-0.4$ or $M_w = 7.05 + 0.95/-0.4$ depending on assumptions
- Our results can be used, for example, to estimate the probability of having an earthquake of or exceeding any magnitude in any timespan

Supporting Information:
- Supporting Information S1

Correspondence to:
C. Rollins,
rollin32@msu.edu

Citation:
Rollins, C., & Avouac, J.-P. (2019). A geodesy- and seismicity-based local earthquake likelihood model for central Los Angeles. *Geophysical Research Letters*, *46*, 3153–3162. https://doi.org/10.1029/2018GL080868

Received 10 OCT 2018
Accepted 21 FEB 2019
Accepted article online 27 FEB 2019
Published online 21 MAR 2019

Abstract We estimate time-independent earthquake likelihoods in central Los Angeles using a model of interseismic strain accumulation and the 1932–2017 seismic catalog. We assume that on the long-term average, earthquakes and aseismic deformation collectively release seismic moment at a rate balancing interseismic loading, mainshocks obey the Gutenberg-Richter law (a log linear magnitude-frequency distribution [MFD]) up to a maximum magnitude and a Poisson process, and aftershock sequences obey the Gutenberg-Richter and "Båth" laws. We model a comprehensive suite of these long-term systems, assess how likely each system would be to have produced the MFD of the instrumental catalog, and use these likelihoods to probabilistically estimate the long-term MFD. We estimate $M_{max} = 6.8 + 1.05/-0.4$ (every ~300 years) or $M_{max} = 7.05 + 0.95/-0.4$ assuming a truncated or tapered Gutenberg-Richter MFD, respectively. Our results imply that, for example, the (median) likelihood of one or more $M_w \geq 6.5$ mainshocks is 0.2% in 1 year, 2% in 10 years, and 18–21% in 100 years.

Plain Language Summary We develop a method to estimate the long-term-average earthquake hazard in a region and apply it to central Los Angeles. We start from an estimate of how quickly faults are being loaded by the gradual bending of the crust and assume that on the long-term average, they should release strain in earthquakes at this same total loading rate. We then use a well-established rule that for every $M_w > 7$ earthquake, there are about ten $M_w > 6$ earthquakes, a hundred $M_w > 5$ earthquakes, and so on (with some variability from an exact 1-10-100 slope), and we assume that there is a maximum magnitude that earthquakes do not exceed. We use these constraints to build long-term earthquake rate models for central LA and then evaluate each model by assessing whether an earthquake system obeying it would have produced the relative rates of small, moderate, and large earthquakes in the 1932–2017 earthquake catalog. We estimate a maximum magnitude of $M_w = 6.8 + 1.05/-0.4$ (every ~300 years) or $M_w = 7.05 + 0.95/-0.4$ in central LA depending on specific assumptions. Our results imply that, for example, "median" likelihood of one or more $M_w \geq 6.5$ mainshocks in central LA is 0.2% in 1 year, 2% in 10 years, and 18–21% in 100 years.

1. Introduction

The transpressional Big Bend of the San Andreas Fault (Figure 1c) induces north-south tectonic shortening across Los Angeles (LA) that is released in thrust earthquakes such as the damaging 1971 $M_w \sim 6.7$ Sylmar, 1987 $M_w \sim 5.9$ Whittier Narrows, and 1994 $M_w = 6.7$ Northridge shocks (e.g., Dolan et al., 1995). Paleoseismologic studies have also found evidence of possible Holocene $M_w \geq 7.0$ earthquakes on several thrust faults in greater LA (Leon et al., 2007, 2009; Rubin et al., 1998; Figure 1a). In principle, one can quantify the likelihoods of future earthquakes on these faults by using geodetic data to assess how quickly elastic strain is accumulating on them and employing the elastic rebound hypothesis (Field et al., 2015; Reid, 1910), which implies that they should release strain at this same rate on the long-term average. The strain accumulation can also be expressed as a deficit of seismic moment, which can be assumed to be balanced over the long term by the moment released in earthquakes and aseismic slip (Avouac, 2015; Brune, 1968; Molnar, 1979). This approach has found use in several regional and global studies (e.g., Hsu et al., 2016; Michel et al., 2018; Rong et al., 2014; Shen et al., 2007; Stevens & Avouac, 2016, 2017).

Applying this approach to LA is challenging, in part because the task of assessing strain buildup rates encounters several unique hurdles there: some of the thrust faults are blind (do not break the surface), obscuring strain accumulation on them (Lin & Stein, 1989; Shaw & Suppe, 1996; Stein & Yeats, 1989); the geodetic data are affected by deformation related to aquifer and oil use (Argus et al., 2005; Riel et al., 2018); and central LA sits atop a deep sedimentary basin that introduces a first-order elastic heterogeneity

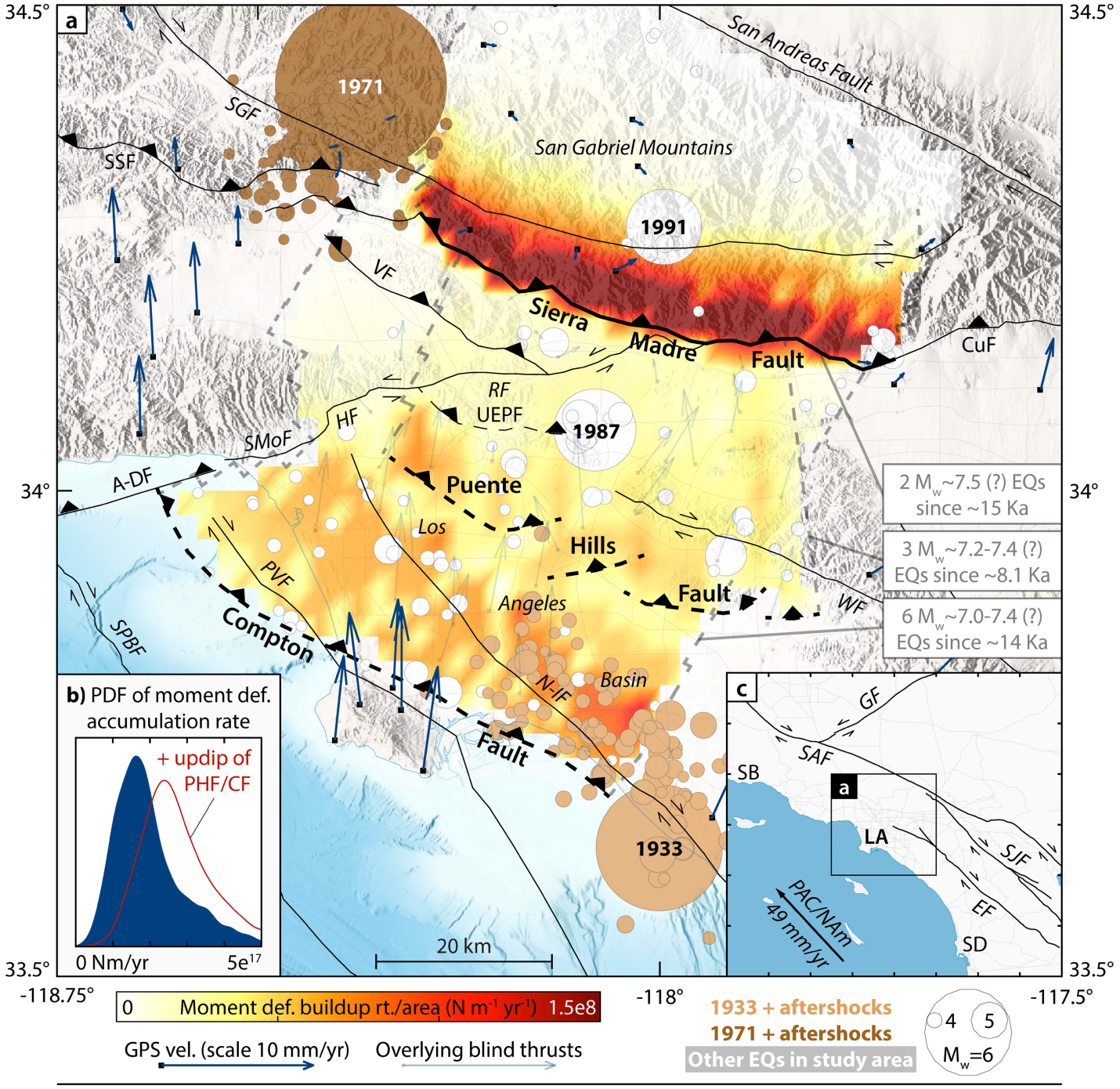

Figure 1. (a) N-S shortening, seismic moment deficit buildup, and earthquakes in central LA. The blue arrows (translucent in study area) are Global Positioning System velocities relative to the San Gabriel Mountains corrected for anthropogenic deformation and interseismic locking on the San Andreas system (Argus et al., 2005). Paleoearthquakes on the Sierra Madre, Puente Hills, and Compton faults are respectively from Rubin et al. (1998) and Leon et al. (2007, 2009). The color shading is geodetically inferred distribution of moment deficit buildup rate associated with these three faults (Rollins et al., 2018). Study area is defined by the three faults and an inferred master décollement (thin dashed lines). The 1932–2017 earthquake locations and magnitudes are from the Southern California Earthquake Data Center catalog. The 1933 Long Beach and 1971 Sylmar earthquakes and their aftershocks (brown circles) occurred on the periphery of the study area. The black lines are upper edges of faults, and the dashed lines are for blind faults. Faults: SGF, San Gabriel; SSF, Santa Susana; VF, Verdugo; CuF, Cucamonga; A-DF, Anacapa-Dume; SMoF, Santa Monica; HF, Hollywood; RF, Raymond; UEPF, Upper Elysian Park; ChF, Chino; WF, Whittier; N-IF, Newport-Inglewood; PVF, Palos Verdes; SPBF, San Pedro Basin. (b) Probability density function (PDF) of moment deficit buildup rate from Rollins et al. (2018). Folding updip of the Puente Hills and Compton faults is assumed anelastic; if it were elastic, the PDF would be the red curve. (c) Tectonic setting. The arrow pairs show slip senses of major faults. Offshore arrow is Pacific Plate velocity relative to North American plate (Kreemer et al., 2014). SB, Santa Barbara. LA, Los Angeles. SD, San Diego. Faults: GF, Garlock; SJF, San Jacinto; EF, Elsinore.

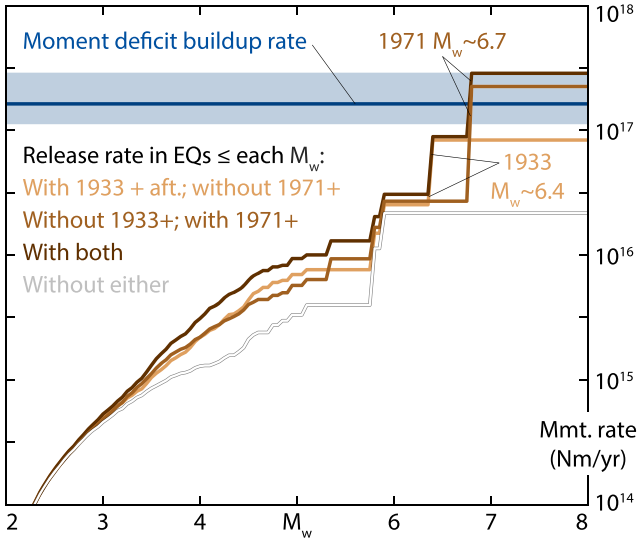

Figure 2. Comparison, over the 86-year timespan of the Southern California Earthquake Data Center catalog, of moment deficit buildup rate (mode and 16th–84th percentiles of probability density function) with moment release rate in earthquakes in Figure 1. The brown and white lines denote, at each magnitude, the cumulative moment release per year by earthquakes that do not exceed that magnitude. We consider four versions of the instrumental catalog as indicated. aft.: aftershocks.

(Shaw et al., 2015). In recent work, Rollins et al. (2018) addressed these three challenges and modeled the north-south shortening as resulting from interseismic strain buildup on the upper sections of the north dipping Sierra Madre, Puente Hills, and Compton thrust faults (Figure 1a), implying that a deficit of seismic moment accrues at a total rate of $1.6 + 1.3/-0.5 \times 10^{17}$ Nm/year (Figure 1b). This model assumes that deformation updip of the blind Compton and Puente Hills faults is anelastic and aseismic; the total moment deficit buildup rate would be $2.4 + 1.3/-0.6 \times 10^{17}$ Nm/year if this deformation were instead elastic (Figure 1b), but this seems unlikely in view of the depth distribution of seismicity (Rollins et al., 2018). The 1.6×10^{17} Nm/year moment deficit could be all released by a $M_w = 7.0$ earthquake every 240 years, for example, but this cannot form a basis for seismic hazard assessment as (1) the choice of magnitude is arbitrary and (2) it overlooks the contributions of smaller (and possibly larger) events and aseismic slip. Here we develop a probabilistic estimate of long-term-average earthquake likelihoods by magnitude in central LA that accounts for these factors, using the moment deficit buildup rate and the seismic catalog.

2. Moment Buildup Versus Release in Earthquakes

We first assess whether this moment deficit has been balanced by the collective moment release in small, moderate, and large earthquakes over the period of the instrumental catalog (e.g., Meade & Hager, 2005; Stevens & Avouac, 2016). We use locations and magnitudes from the 1932–2017 Southern California Earthquake Data Center (SCEDC) catalog within a study area defined by the geometries of the Sierra Madre, Puente Hills, and Compton faults and an inferred master décollement (Fuis et al., 2001; Shaw et al, 2015; Rollins et al., 2018; Figure 1a, thin dashed lines). The 1933 M_w ~ 6.4 Long Beach and 1971 M_w ~ 6.7 Sylmar earthquakes occurred on the edges of the study area (Figure 1a); we handle this ambiguity by using four versions of the instrumental catalog that alternatively include or exclude them and their aftershocks (supporting information S1). (We exclude the 1994 Northridge earthquake, which occurred further west on a fault not counted in our estimate of moment deficit buildup rate.) We compare moment buildup and release in 1932–2017 over a range of upper cutoff magnitudes for the earthquakes so as to qualitatively assess how large earthquakes need to get in central LA to collectively balance the "moment budget". The answer visibly depends on whether the 1933 and 1971 earthquakes are counted or not (Figure 2). This technical issue hints at the reason why this comparison has limited predictive power: the instrumental catalog (e.g., exactly one M_w ~ 6.4 and one M_w ~ 6.7 earthquake) does not simply repeat every 86 years but rather is an 86-year realization of an underlying process. (This approach also ignores the moment released by undetected small earthquakes, which may be nonnegligible.)

3. The Gutenberg-Richter Relation, Long-Term Models, and a New Approach

A way around these issues is to assume that on the long-term average, (1) the geodetic moment deficit buildup rate is constant and is balanced by earthquakes and aseismic deformation and (2) earthquakes obey the Gutenberg-Richter (G-R) law, meaning that their magnitude-frequency distribution (MFD) is log linear with slope $-b$ (Gutenberg & Richter, 1954). If the G-R distribution is additionally assumed to hold up to a maximum earthquake magnitude M_{max}, the long-term MFD is uniquely determined by the moment buildup rate, b, M_{max}, and the aseismic contribution (Avouac, 2015; Molnar, 1979). We work with two alternate closed-form MFD solutions: a truncated G-R distribution (supporting information S2) and a *tapered* G-R distribution (supporting information S3). In the 2-D space of M_w versus log-frequency of earthquakes of or exceeding that M_w, which we call G-R space, the truncated G-R distribution is a line that ends at M_{max} (Figures S1a and S1 S2a), while the tapered G-R distribution tapers to $-\infty$ at M_{max} (Figures S1c and S2f). These may be suitable end-members: the truncated G-R distribution in fact implies a mix of log linear and characteristic behavior (Figure S1a and supporting information S2); the tapered G-R distribution (which

implies no characteristic element) follows from a different use of the log linear relation (supporting information S3) and does not require specifying a form for the tapering (e.g., Jackson & Kagan, 1999), and both are log linear in G-R space except at or near M_{max} and therefore may be reconcilable with observations in most settings.

However, several challenges remain in this approach. First, M_{max} is unknown due to the short history of observation. Some studies iteratively estimate M_{max} in cumulative magnitude-frequency space (Stevens & Avouac, 2016, 2017); others estimate it using total fault areas and scaling relations (Field et al., 2014) or assume a value for the maximum earthquake's recurrence interval (Hsu et al., 2016). Second, while some studies estimate b a priori from the catalog (Field et al., 2014; Stevens & Avouac, 2016, 2017), it is desirable to fully account for the covariances between b, M_{max}, the moment deficit buildup rate, and other factors in estimating long-term earthquake rates. Third, it is uncertain whether to decluster the instrumental catalog first (Michel et al., 2018), which method to use if so, whether declustering should yield a smaller b-value (Felzer, 2007; Marsan & Lengline, 2008), and how this may affect the inferred long-term model.

Here we develop a probabilistic method to estimate long-term earthquake rates in a way that handles these challenges (Figures S1 and S2 and supporting information S2–S5). We generate a large suite of moment-balancing long-term models (described by MFDs), use each to populate a set of synthetic 86-year earthquake catalogs, and compare the synthetic MFDs to that of the 86-year-long SCEDC catalog to evaluate how likely the 1932–2017 seismicity would be to arise as an 86-year realization of each long-term process. This approach is similar to the "Turing-style" tests of Page and van der Elst (2018). We generate the long-term models by iterating over a wide range of values of b and M_{max} and over the probability density function (PDF) of moment deficit accumulation rate (Figure 1b) and computing the moment-balancing truncated or tapered G-R MFD under each combination of parameters (supporting information S2 and S3). Following Michel et al. (2018), we incorporate "Båth's law," the observation that the largest aftershock is often ~1.2 magnitude units smaller than the mainshock (Båth, 1965). To do so, we assume that it is mainshocks (not all earthquakes) that obey the truncated or tapered G-R form described by b and that each mainshock is then individually accompanied by aftershocks obeying their own truncated G-R distribution (described by the same b) up to a single aftershock 1.2 magnitude units below the mainshock. The moment contribution of aftershocks is then a constant (supporting information S4), and the parameter b is essentially the "declustered" (mainshocks-only) b-value, which we have also assumed governs individual aftershock sequences. We assume that each mainshock is also followed by aseismic deformation that releases 25% as much moment as the mainshock, based on inferences from the Northridge earthquake (Donnellan & Lyzenga, 1998). We then use each long-term MFD to populate a set of 25 synthetic 86-year catalogs assuming that mainshocks of each magnitude obey a Poisson process and adding their aftershocks. We compute the misfit of the 25 synthetic catalogs' cumulative MFDs to those of the four versions of the 1932–2017 catalog in G-R space (Figures S2b–S2d), convert these misfits to Gaussian likelihoods, and use these likelihoods to compute the PDFs of key parameters and long-term earthquake rates (supporting information S5). In a truncated G-R distribution, these parameters also define T (M_{max}), the maximum earthquake's recurrence interval, so we estimate the 2-D PDF of M_{max} and T (M_{max}); in a tapered G-R distribution, T (M_{max}) is infinite and so we only estimate the 1-D PDF of M_{max}. This method has the advantages that (1) it directly tests long-term models based on whether the instrumental catalog is a plausible realization of each long-term process, (2) b and M_{max} are estimated a posteriori with full covariance with other variables, and 3) it does not require declustering the catalog.

4. Results

We first describe our two preferred long-term average earthquake likelihood models (Figure 3), which respectively assume a truncated and a tapered G-R distribution for mainshocks. In the truncated case, the 2-D PDF of M_{max} and T (M_{max}) peaks at a $M_w = 6.75$ event with a recurrence interval of ~280 years. The weighted 16th- and 84th-percentile recurrence intervals of the maximum earthquake for $M_{max} = 6.75$ are 170 and 610 years; the 1-D PDF of M_{max} (mode and same percentiles) is $M_w = 6.8 + 1.05/-0.4$ (Figure 3a). In the tapered case, the 1-D PDF of M_{max} gives $M_w = 7.05 + 0.95/-0.4$. (M_{max} is always ~0.25 larger in the tapered models because the tapering requires a larger M_{max} to close the moment budget.) The aggregate mean magnitude and recurrence interval of paleoseismologically inferred Holocene

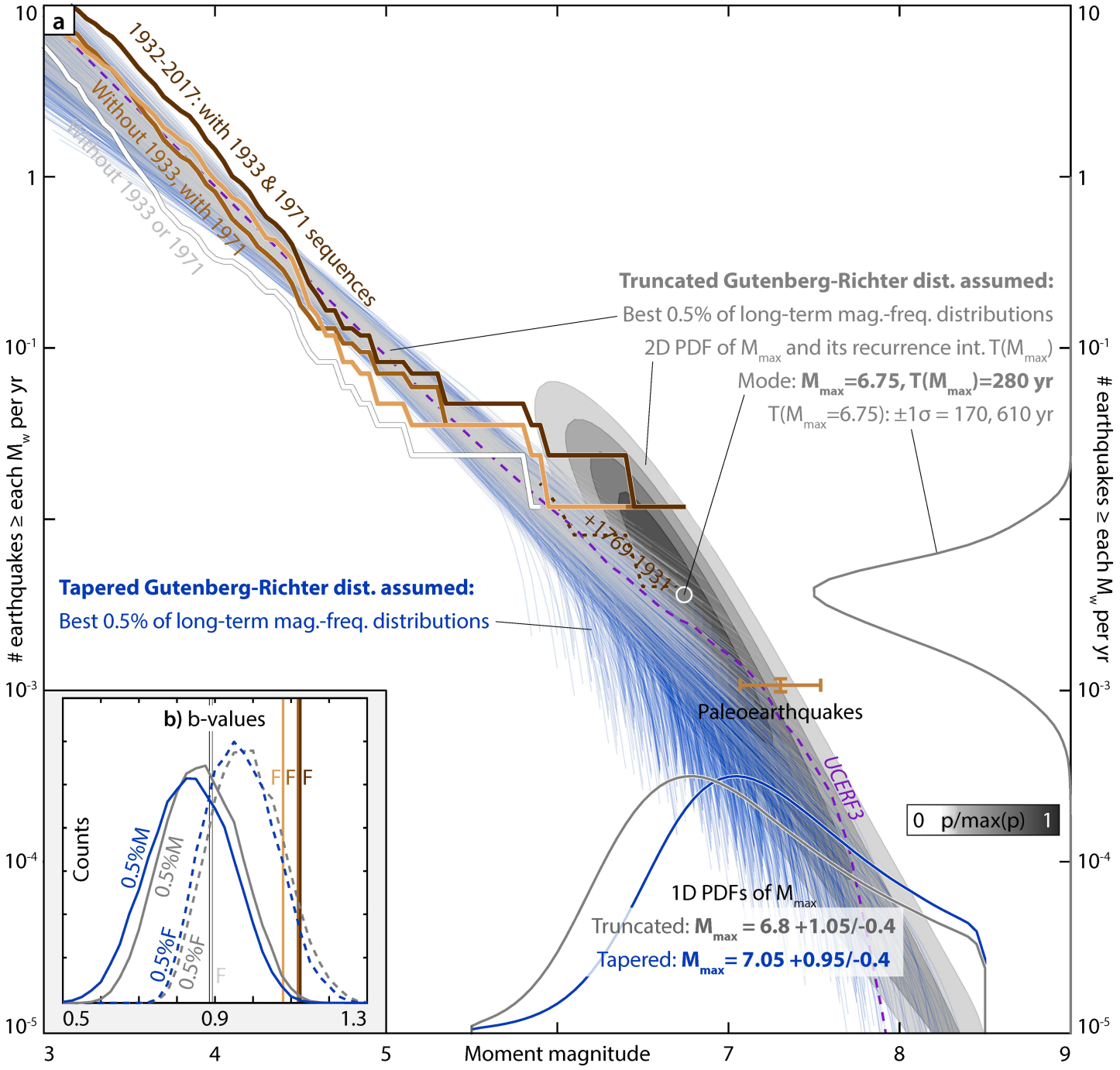

Figure 3. (a) Preferred estimates of long-term-average earthquake likelihoods (in Gutenberg-Richter space), assuming that mainshocks obey a truncated (gray) or tapered (blue) Gutenberg-Richter (G-R) magnitude-frequency distribution (MFD) and are accompanied by aftershocks obeying a truncated G-R MFD and "Båth's law" plus postseismic deformation. The brown lines are cumulative MFDs of the four versions of the instrumental catalog. Thin translucent lines are full MFDs (including aftershocks) of the best fit ting 0.5% of models in the truncated (gray) and tapered (blue) cases. The gray shape is the 2-D probability density function (PDF) of the maximum earthquake's magnitude and recurrence interval assuming a truncated G-R distribution. The brown error bars show aggregate recurrence interval and magnitudes of paleoearthquakes in Figure 1. The dashed purple line is cumulative UCERF3 nucleation MFD from all faults in study area (supporting information S7). (b) Histograms of *b*-values in the best fitting 0.5% of truncated (gray) and tapered (blue) models. The solid lines are intrinsic model parameter *b* that governs mainshocks (*M*) and individual aftershock sequences; the dashed lines are maximum-likelihood (Aki, 1965) *b*-values of the full (*F*) long-term MFDs of the same models (including aftershocks) at $M_c = 3.5$; the brown lines are maximum-likelihood *b*-values of four versions of the instrumental catalog at $M_c = 3.5$.

earthquakes on the Sierra Madre, Puente Hills, and Compton faults are respectively $M_w = 7.31 \pm 0.24$ and 920 + 100/−80 years (Figure 3a, brown error bars). While our PDFs for M_{max} peak at smaller magnitudes, they do not exclude the possibility of such large earthquakes: the likelihood of M_{max} being $\geq M_w = 7.3$ is respectively 38% and 47% in the truncated and tapered estimates. (The paleomagnitudes were also estimated using scaling relations based on both strike-slip and thrust earthquakes and would be ~0.5 lower if relations based only on thrust earthquakes were used (Leon et al., 2009).) In both estimates, the full MFDs (including aftershocks) of the lowest misfit long-term-average models (Figure 3a, thin translucent gray and blue lines) are comparable to the instrumental MFDs at smaller magnitudes (brown lines). The "lowest-misfit" full MFDs are also comparable to the sum of the cumulative nucleation MFDs on all faults in the study area from the Uniform California Earthquake Rupture Forecast, Version 3 (UCERF3; Field et al., 2014; Figure 3a, dashed purple line; supporting information S7) except that the UCERF3 MFD goes to higher magnitudes (see section 6). The intrinsic model parameter b (governing mainshocks) in the lowest misfit models peaks at 0.8–0.9 (Figure 3b, solid blue and gray lines), close to the statewide declustered value of $b = 0.85 \pm 0.13$ (Felzer, 2007). The maximum-likelihood ($M_c = 3.5$) effective b-values of the full long-term MFDs (including aftershocks) in the lowest misfit models peak at 0.9–1.0 (Figure 3b, dashed blue and gray), consistent with the maximum-likelihood b-values of the four versions of the instrumental catalog (Figure 3b, brown lines) and with the Hutton et al. (2010) estimate of $b \approx 1.0$ for Southern California. The effective b-values may peak slightly below 1.0 because the aftershock sequences of the 1987 Whittier Narrows and 1991 $M_w \sim 5.8$ Sierra Madre earthquakes had respective b-values of 0.67 and 0.6 (Hauksson, 1994; Hauksson & Jones, 1989) and are in all four versions of the instrumental catalog constraining these models.

These preferred models apply equal weighting to the four versions. We assess the effect of this by generating four alternate estimates each calibrated to only one version. We find that the version used has a substantial but intuitive effect on M_{max}. The version that excludes the 1933 and 1971 events and their aftershocks features relatively low earthquake rates (and fell far short of balancing the 86-year moment budget on its own; Figure 2, white line), and so the model must add more large, infrequent earthquakes to balance the long-term-average moment budget: $M_{max} = 7.15 + 1.0/-0.45$ and $M_{max} = 7.3 + 0.9/-0.35$ for the truncated and tapered cases, respectively (Figure S3d). The subcatalog that counts both the 1933 and 1971 sequences, by contrast, features much higher small and moderate earthquake rates and so large earthquakes are not needed in the long-term moment budget: $M_{max} = 6.4 + 1.05/-0.2$ (truncated) and $M_{max} = 6.65 + 0.95/-0.3$ (tapered; Figure S3a). The estimates using versions that count one sequence or the other lie in the middle of these two, as might be expected (Figures S3b and S3c).

If we assume that postseismic deformation is nonexistent and 100% of moment release occurs in earthquakes, larger earthquakes are needed to close the moment budget: $M_{max} = 6.95 + 1.05/-0.45$ (truncated) and $M_{max} = 7.2 + 0.85/-0.45$ (tapered; Figure S4a). If we alternatively assume that strain accumulation updip of the Puente Hills and Compton faults is elastic, the moment deficit buildup is ~50% faster (Figure 1b, red line) and so $M_{max} = 7.1 + 0.95/-0.4$ (truncated) and $M_{max} = 7.35 + 0.8/-0.45$ (tapered; Figure S4b). We can also relax the mainshock-aftershock distinction and assume instead that all earthquakes obey a single G-R distribution characterized by the intrinsic parameter b (which is then the b-value of the full MFD) and Poisson recurrence. This yields a similar long-term model, with $M_{max} = 6.9 + 1.05/-0.45$ (truncated) and $M_{max} = 7.15 + 0.9/-0.5$ (tapered; Figure S5a), and $b = 0.9$–1.0 in the lowest-misfit models (Figure S5b), consistent with the maximum-likelihood full b-value in the preferred models (Figure 3b).

5. Implications for Earthquake Likelihoods in LA

Our preferred models (Figure 3) can be used, for example, to estimate the likelihood of observing at least one mainshock of at least a given magnitude in a given time period (supporting information S6). Assuming that mainshocks of each magnitude follow a Poisson process, the weighted-median probability of observing at least one $M_w \geq 6.0$ mainshock is 59% in 100 years, 8.5% in 10 years, and 0.9% in 1 year for the truncated G-R model or 62% in 100 years, 9.3% in 10 years, and 1.0% in 1 year for the tapered model (Figure 4). The likelihoods are similar if one assumes that mainshocks follow a Brownian renewal process (Field & Jordan, 2015; Matthews et al., 2002; Figure S6). The weighted-median probabilities of at least one $M_w \geq 6.5$ mainshock assuming a Poisson process are 18% in 100 years, 2.0% in 10 years, and 0.2% in 1 year (truncated) or 21%, 2.3%, and 0.2% (tapered). The probability of observing three or more $M_w \geq 5.9$

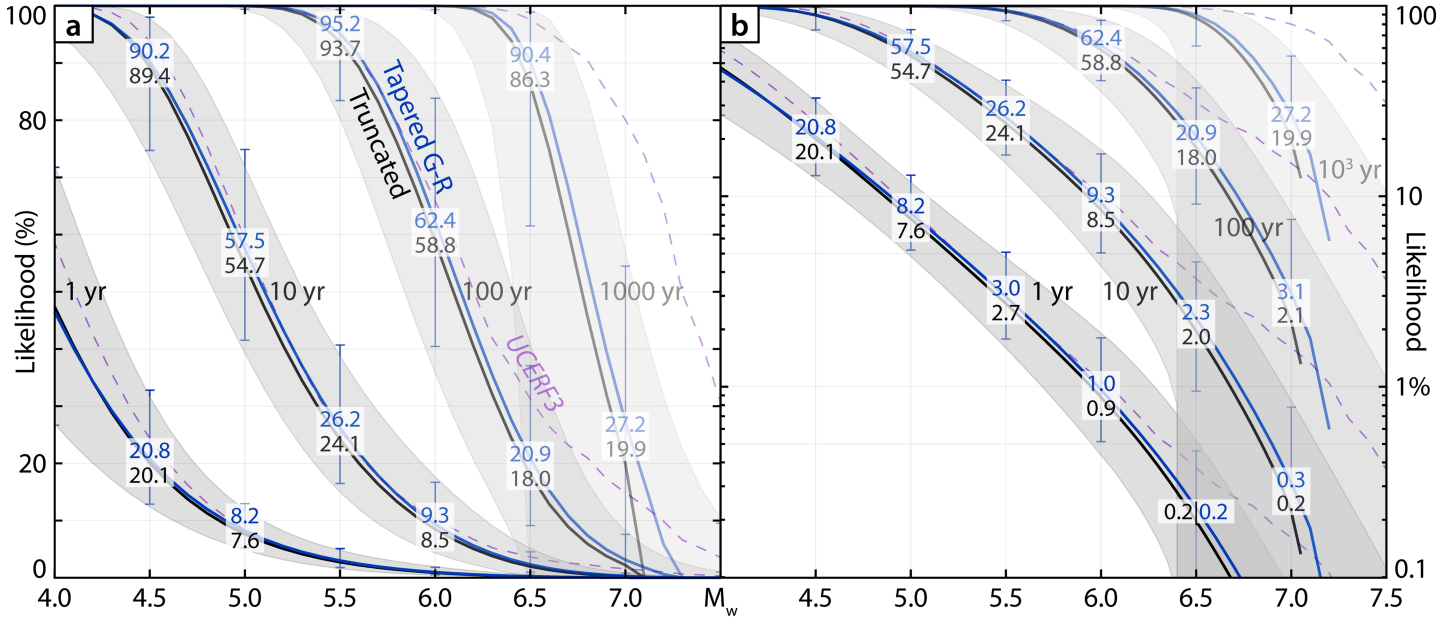

Figure 4. Likelihoods (plotted with a (a) linear or (b) logarithmic *y* axis) of observing at least one mainshock of or exceeding a given magnitude in the study area over a 1-, 10-, 100-, or 1,000-year period as indicated, assuming that individual mainshocks obey a Poisson process. The gray lines and shading are weighted median and weighted 16th–84th-percentile likelihoods assuming a truncated G-R distribution. The blue lines and error bars are the same assuming a tapered G-R distribution. Dashed purple lines show Poisson likelihoods from the UCERF3 MFD in Figure 3.

mainshocks in 86 years is 7.5% (truncated) or 9.4% (tapered), suggesting that it is rather unlikely to have observed three earthquakes like the M_w ~ 6.7 Sylmar, M_w ~ 6.4 Long Beach, and M_w ~ 5.9 Whittier Narrows shocks in the 86-year instrumental period. Even counting aftershocks, the rates of earthquakes of or exceeding those magnitudes are still several times lower in these models than in the catalog (Figure 3a). In order words, according to these models, central LA has experienced a relative abundance of $M_w \geq 5.9$ earthquakes in the instrumental era. We note that the instrumental era may have followed a relatively quiet period (although incompleteness issues make this somewhat speculative): Toppozada and Branum (2002) reports only two $M_w \geq 6$ earthquakes in central LA between 1769 and 1932, and one of them, the 1769 earthquake felt by the Portola expedition, may have in fact occurred in Orange County (Grant et al., 2002), leaving only a M ~ 6 earthquake in 1855 in the study area (Yerkes, 1985). If one downward-adjusts the instrumental MFD above $M_w = 5.9$ by adding only one $M_w = 6.0$ earthquake in 163 years, the total MFD (Figure 3a, dashed brown line) more closely matches our long-term model and the UCERF3 nucleation MFD. If one adds this quiescence to the entire instrumental MFD and then reruns our method, M_{max} rises to $M_w = 7.15 + 0.85/-0.4$ (truncated) or $M_w = 7.45 + 0.65/-0.45$ (tapered; Figure S4c).

6. Discussion/Conclusion

Our method for probabilistically estimating long-term earthquake likelihoods satisfies the moment conservation principle, accounts for a broad range of data and considerations, and can be used in probabilistic seismic hazard assessment anywhere. It has features in common with relatively successful existing forecasts, such as the separation of mainshocks and aftershocks (Helmstetter et al., 2007), use of geodetic data (Bird et al., 2015; Field et al., 2014), and model tuning based on retrospective prediction of seismic catalogs (Bird et al., 2015; Page & van der Elst, 2018). However, our approach has the advantage of estimating *b*, M_{max}, and long-term earthquake likelihoods a posteriori with full covariance. Our results may not be unreasonable: an earthquake rupturing the entire Sierra Madre Fault, for example, would have magnitude $M = 7.26$ or $M = 7.40$ using empirical scaling relations from Wells and Coppersmith (1994; thrust events only) or Hanks and Bakun (2008), respectively. This is similar to our $M_{max} = 7.2 + 0.85/-0.45$ tapered G-R estimate assuming 100% of slip occurs seismically (Figure S4a) even though these scaling relations

are independent of strain buildup (and we infer that the Sierra Madre Fault is not likely locked over its full area (Rollins et al., 2018).)

Several caveats are nevertheless worth noting. First, our approach is not only time-independent (it does not incorporate the time distribution of earthquakes in the SCEDC catalog, for example) but also operates on long-term averages. Even if the estimated PDF of M_{max} and T (M_{max}) were a 2-D delta function at $M_w = 6.75$ and 280 years, for example, this would not imply that larger earthquakes should never occur, only that they would likely overshoot the moment budget (given the rest of the model) and should on average be balanced by relative quiescence. The timescale over which this balance may exist is unknown, as large earthquakes may cluster in time over thousands of years (Benedetti et al., 2013; Dolan et al., 2007; McCalpin & Nishenko, 1996; Rockwell et al., 2000), and so the large inferred paleoearthquakes could also be features of a system of which our models are a long-term average. Second, we assume that interseismic deformation rates are time-independent, which may be untrue (e.g., Mavrommatis et al., 2014; Tsang et al., 2015). Third, we assume that all earthquakes are either inside or outside the study area, which belies the possibility of a large earthquake rupturing faults both within central LA and outside it. Fourth, we also implicitly assume that the earthquakes only release strain from north-south shortening; although this is the principal strain in LA (Zoback et al., 1987), it is only a component of the relative plate motion. These two factors may explain why the cumulative local UCERF3 nucleation MFD has a larger M_{max} than our preferred model (Figure 3b). (In UCERF2, which did not incorporate multifault ruptures, the inferred M_{max} on the Sierra Madre and Puente Hills faults was ~0.5 lower; Field et al., 2007). Fifth, while the truncated G-R distribution does imply an element of characteristic behavior at M_{max} (Figure S1a, supporting information S2), which we find lowers the estimated M_{max} by ~0.25 compared to the tapered distribution, we do not explore more characteristic MFDs like those inferred by UCERF3. Finally, our method would require adjustment (and denser geodetic data or other constraints) in order to be separable into single-fault forecasts (e.g., Field et al., 2014).

Acknowledgments

C. Rollins was supported by a NASA Earth and Space Science Fellowship for most of this work. The authors are grateful to Tom Parsons and an anonymous reviewer for suggestions that greatly improved the manuscript, as well as numerous colleagues around the community for helpful input and guidance. The authors declare no competing financial interests. The GPS data used to constrain the moment deficit buildup rate in Rollins et al. (2018) and plotted in Figure 1 can be found in Argus et al. (2005, Table 3); the SCEDC seismic catalog is available at http://service.scedc.caltech.edu/ftp/catalogs/SCEC_DC/.

References

Aki, K. (1965). Maximum likelihood estimate of b in the formula $\log N = a - bM$ and its confidence limits. *Bulletin of the Seismological Society of America*, *43*, 237–239.

Argus, D. F., Heflin, M. B., Peltzer, G., Crampé, F., & Webb, F. H. (2005). Interseismic strain accumulation and anthropogenic motion in metropolitan Los Angeles. *Journal of Geophysical Research*, *110*, B04401. https://doi.org/10.1029/2003JB002934

Avouac, J.-P. (2015). From geodetic imaging of seismic and aseismic fault slip to dynamic modeling of the seismic cycle. *Annual Review of Earth and Planetary Sciences*, *43*(1), 233–271. https://doi.org/10.1146/annurev-earth-060614-105302

Båth, M. (1965). Lateral inhomogeneities of the upper mantle. *Tectonophysics*, *2*(6), 483–514. https://doi.org/10.1016/0040-1951(65)90003-X

Benedetti, L., Manighetti, I., Gaudemer, Y., Finkel, R., Malavieille, J., Pou, K., et al. (2013). Earthquake synchrony and clustering on Fucino faults (Central Italy) as revealed from in situ 36Cl exposure dating. *Journal of Geophysical Research: Solid Earth*, *118*, 4948–4974. https://doi.org/10.1002/jgrb.50299

Bird, P., Jackson, D. D., Kagan, Y. Y., Kreemer, C., & Stein, R. S. (2015). GEAR1: A global earthquake activity rate model constructed from geodetic strain rates and smoothed seismicity. *Bulletin of the Seismological Society of America*, *105*(5), 2538–2554. https://doi.org/10.1785/0120150058

Brune, J. N. (1968). Seismic moment, seismicity, and rate of slip along major fault zones. *Journal of Geophysical Research*, *73*(2), 777–784. https://doi.org/10.1029/JB073i002p00777

Dolan, J. F., Bowman, D. D., & Sammis, C. G. (2007). Long-range and long-term fault interactions in Southern California. *Geology*, *35*(9), 855–858.

Dolan, J. F., Sieh, K., Rockwell, T. K., Yeats, R. S., Shaw, J., Suppe, J., et al. (1995). Prospects for larger or more frequent earthquakes in the Los Angeles metropolitan region. *Science*, *267*(5195), 199–205. https://doi.org/10.1126/science.267.5195.199

Donnellan, A., & Lyzenga, G. A. (1998). GPS measurements of fault afterslip and upper crustal deformation following the Northridge earthquake. *Journal of Geophysical Research*, *103*(B9), 21285–21297. https://doi.org/10.1029/98JB01487

England, P., & Bilham, R. (2015). The Shillong Plateau and the great 1897 Assam earthquake. *Tectonics*, *34*, 1792–1812. https://doi.org/10.1002/2015TC003902

Felzer, K. R. (2007). Appendix I: Calculating California Seismicity Rates. In "The Uniform California Earthquake Rupture Forecast, Version 2 (UCERF2)." USGS Open-File Report 2007-1437I.

Field, E. H., Arrowsmith, R. J., Biasi, G. P., Bird, P., Dawson, T. E., Felzer, K. R., et al. (2014). Uniform California earthquake rupture forecast, version 3 (UCERF3)—The time-independent model. *Bulletin of the Seismological Society of America*, *104*(3), 1122–1180. https://doi.org/10.1785/0120130164

Field, E. H., Biasi, G. P., Bird, P., Dawson, T. E., Felzer, K. R., Jackson, D. D., et al. (2015). Long-term time-dependent probabilities for the Third Uniform California Earthquake Rupture Forecast (UCERF3). *Bulletin of the Seismological Society of America*, *105*(2A), 511–543. https://doi.org/10.1785/0120140093

Field, E. H., Dawson, T. E., Felzer, K. R., Frankel, A., Gupta, P., Jordan, T. H., et al. (2007). The Uniform California Earthquake Rupture Forecast, Version 2 (UCERF2). USGS Open-File Report 2007-1437I.

Field, E. H., & Jordan, T. H. (2015). Time-dependent renewal-model probabilities when date of last earthquake is unknown. *Bulletin of the Seismological Society of America*, *105*(1), 459–463. https://doi.org/10.1785/0120140096

Fuis, G., Ryberg, T., Godfrey, N., Okaya, D., & Murphy, J. (2001). Crustal structure and tectonics from the Los Angeles basin to the Mojave Desert, southern California. *Geology*, *29*(1), 15–18. https://doi.org/10.1130/0091-7613(2001)029<0015:CSATFT>2.0.CO;2

Grant, L. B., Ballenger, L. J., & Runnerstrom, E. E. (2002). Coastal uplift of the San Joaquin Hills, southern Los Angeles Basin, California, by a large earthquake since AD 1635. *Bulletin of the Seismological Society of America*, *92*(2), 590–599. https://doi.org/10.1785/0120010119

Gutenberg, B., & Richter, C. F. (1954). *Seismicity of the Earth and associated phenomena*. Princeton, N.J: Princeton University Press.

Hanks, T. H., & Bakun, W. H. (2008). M-log a observations for recent large earthquakes. *Bulletin of the Seismological Society of America*, *98*(1), 490–494. https://doi.org/10.1785/0120070174

Hauksson, E. (1994). The 1991 Sierra Madre earthquake sequence in southern California: Seismological and tectonic analysis. *Bulletin of the Seismological Society of America*, *84*(4), 1058–1074.

Hauksson, E., & Jones, L. M. (1989). The 1987 Whittier narrows earthquake sequence in Los Angeles, Southern California, seismological and tectonic analysis. *Journal of Geophysical Research*, *94*(B7), 9569–9589. https://doi.org/10.1029/JB094iB07p09569

Hauksson, E., Yang, W., & Shearer, P. M. (2012). Waveform relocated earthquake catalog for southern California (1981 to June 2011). *Bulletin of the Seismological Society of America*, *102*(5), 2239–2244. https://doi.org/10.1785/0120120010

Helmstetter, A., Kagan, Y. Y., & Jackson, D. D. (2007). High-resolution time-independent grid-based forecast for $M \geq 5$ earthquakes in California. *Seismological Research Letters*, *78*(1), 78–86. https://doi.org/10.1785/gssrl.78.1.78

Hsu, Y.-J., Yu, S.-B., Loveless, J. P., Bacolcol, T., Solidum, R., Luis, A. Jr., et al. (2016). Interseismic deformation and moment deficit along the Manila subduction zone and the Philippine Fault system. *Journal of Geophysical Research: Solid Earth*, *121*, 7639–7665. https://doi.org/10.1002/2016JB013082

Hutton, K., Woessner, J., & Hauksson, E. (2010). Earthquake monitoring in southern California for seventy-seven years (1932–2008). *Bulletin of the Seismological Society of America*, *100*(2), 423–446. https://doi.org/10.1785/0120090130

Jackson, D. D., & Kagan, Y. Y. (1999). Testable earthquake forecasts for 1999. *Seismological Research Letters*, *70*(4), 393–403. https://doi.org/10.1785/gssrl.70.4.393

Kreemer, C., Blewitt, G., & Klein, E. C. (2014). A geodetic plate motion and Global Strain Rate Model. *Geochemistry, Geophysics, Geosystems*, *15*, 3849–3889. https://doi.org/10.1002/2014GC005407

Leon, L. A., Christofferson, S. A., Dolan, J. F., Shaw, J. H., & Pratt, T. L. (2007). Earthquake-by-earthquake fold growth above the Puente Hills blind thrust fault, Los Angeles, California: Implications for fold kinematics and seismic hazard. *Journal of Geophysical Research*, *112*, B03S03. https://doi.org/10.1029/2006JB004461

Leon, L. A., Dolan, J. F., Shaw, J. H., & Pratt, T. L. (2009). Evidence for large Holocene earthquakes on the Compton thrust fault, Los Angeles, California. *Journal of Geophysical Research*, *114*, B12305. https://doi.org/10.1029/2008JB006129

Lin, J., & Stein, R. S. (1989). Coseismic folding, earthquake recurrence, and the 1987 source mechanism at Whittier Narrows, Los Angeles Basin, California. *Journal of Geophysical Research*, *94*(B7), 9164–9632.

Marsan, D., & Lengline, O. (2008). Extending earthquakes' reach through cascading. *Science*, *319*(5866), 1076–1079. https://doi.org/10.1126/science.1148783

Marshall, S. T., Cooke, M. L., & Owen, S. E. (2009). Interseismic deformation associated with three-dimensional faults in the greater Los Angeles region, California. *Journal of Geophysical Research*, *114*, B12403. https://doi.org/10.1029/2009JB006439

Marshall, S. T., Funning, G. J., & Owen, S. E. (2013). Fault slip rates and interseismic deformation in the western Transverse Ranges, California. *Journal of Geophysical Research: Solid Earth*, *118*, 4511–4534. https://doi.org/10.1002/jgrb.50312

Matthews, M. V., Ellsworth, W. L., & Reasenberg, P. A. (2002). A Brownian model for recurrent earthquakes. *Bulletin of the Seismological Society of America*, *92*(6), 2233–2250. https://doi.org/10.1785/0120010267

Mavrommatis, A. P., Segall, P., & Johnson, K. M. (2014). A decadal-scale deformation transient prior to the 2011 Mw9.0 Tohoku-oki earthquake. *Geophysical Research Letters*, *41*, 4486–4494. https://doi.org/10.1002/2014GL060139

McCalpin, J., & Nishenko, S. (1996). Holocene paleoseismicity, temporal clustering, and probabilities of future large ($M > 7$) earthquakes on the Wasatch fault zone, Utah. *Journal of Geophysical Research*, *101*(B3), 6233–6253. https://doi.org/10.1029/95JB02851

Meade, B. J., & Hager, B. H. (2005). Spatial localization of moment deficits in southern California. *Journal of Geophysical Research*, *110*, B04402. https://doi.org/10.1029/2004JB003331

Michel, S., Avouac, J.-P., Jolivet, R., & Wang, L. (2018). Seismic and aseismic moment budget and implication for the seismic potential of the Parkfield Segment of the San Andreas Fault. *Bulletin of the Seismological Society of America*, *108*(1), 19–38. https://doi.org/10.1785/0120160290

Molnar, P. (1979). Earthquake recurrence intervals and plate tectonics. *Bulletin of the Seismological Society of America*, (1), 115–133.

Page, M. T., & van der Elst, N. (2018). Turing-Style Tests for UCERF3 Synthetic Catalogs. *Bulletin of the Seismological Society of America*, *108*(2), 729–741. https://doi.org/10.1785/0120170223

Reid, H. F. (1910). The mechanics of the earthquake. *The California Earthquake of April 18, 1906; Report of the State Investigation Commission* (Carnegie Institution of Washington, Washington, D.C.).

Riel, B. V., Simons, M., Ponti, D., Agram, P., & Jolivet, R. (2018). Quantifying ground deformation in the Los Angeles and Santa Ana coastal basins due to groundwater withdrawal. *Water Resources Research*, *54*, 3557–3582. https://doi.org/10.1029/2017WR021978

Rockwell, T., Lindvall, S., Herzberg, M., Murbach, D., Dawson, T., & Berger, G. (2000). Paleoseismology of the Johnson Valley, Kickapoo, and Homestead Valley faults: Clustering of earthquakes in the eastern California shear zone. *Bulletin of the Seismological Society of America*, *90*(5), 1200–1236. https://doi.org/10.1785/0119990023

Rollins, C., Avouac, J.-P., Landry, W., Argus, D. F., & Barbot, S. D. (2018). Interseismic strain accumulation on faults beneath Los Angeles, California. *Journal of Geophysical Research: Solid Earth*, *123*, 7126–7150. https://doi.org/10.1029/2017JB015387

Rong, Y., Jackson, D. D., Magistrale, H., & Goldfinger, C. (2014). Magnitude limits of subduction zone earthquakes. *Bulletin of the Seismological Society of America*, *104*(5), 2359–2377. https://doi.org/10.1785/0120130287

Rubin, C. M., Lindvall, S. C., & Rockwell, T. K. (1998). Evidence for large earthquakes in metropolitan Los Angeles. *Science*, *281*(5375), 398–402. https://doi.org/10.1126/science.281.5375.398

SCEDC (2013). Southern California Earthquake Data Center (*California Institute of Technology, Pasadena, CA)*. Dataset. https://doi.org/10.7909/C3WD3xH1

Shaw, J. H., & Suppe, J. (1996). Earthquake hazards of active blind-thrust faults under the central Los Angeles basin, California. *Journal of Geophysical Research*, *101*(B4), 8623–8642. https://doi.org/10.1029/95JB03453

Shaw, J. H., Plesch, A., Tape, C., Suess, M. P., Jordan, T. H., Ely, G., et al. (2015). Unified structural representation of the southern California crust and upper mantle. *Earth and Planetary Science Letters*, *415*, 1–15.

Shen, Z. K., Jackson, D. D., & Kagan, Y. Y. (2007). Implications of geodetic strain rate for future earthquakes, with a five-year forecast of M5 earthquakes in Southern California. *Seismological Research Letters*, *78*(1), 116–120. https://doi.org/10.1785/gssrl.78.1.116

Stein, R. S., & Yeats, R. S. (1989). Hidden Earthquakes. *Scientific American*, *260*(6), 48–57. https://doi.org/10.1038/scientificamerican0689-48

Stevens, V., & Avouac, J. P. (2016). Millenary Mw > 9.0 earthquakes required by geodetic strain in the Himalaya. *Geophysical Research Letters*, *43*, 1118–1123. https://doi.org/10.1002/2015GL067336

Stevens, V., & Avouac, J. P. (2017). Determination of M_{max} from background seismicity and moment conservation. *Bulletin of the Seismological Society of America*, *107*(6), 2578–2596. https://doi.org/10.1785/0120170022

Toppozada, T. R., & Branum, D. M. (2002). California $M \geq 5.5$ earthquakes, history and areas damaged. In *International Handbook of Earthquake and Engineering Seismology* (pp. 793–796). Cambridge, MA: Academic Press.

Tsang, L. L. H., Meltzner, A. J., Hill, E. M., Freymueller, J. T., & Sieh, K. (2015). A paleogeodetic record of variable interseismic rates and megathrust coupling at Simeulue Island, Sumatra. *Geophysical Research Letters*, *42*, 10,585–10,594. https://doi.org/10.1002/2015GL066366

Wells, D. L., & Coppersmith, K. J. (1994). New empirical relationships among magnitude, rupture length, rupture width, rupture area, and surface displacement. *Bulletin of the Seismological Society of America*, *84*(4), 974–1002.

Yerkes, R. F. (1985). Geologic and seismologic setting. In *Evaluating earthquake hazards in the Los Angeles Region—An Earth-science perspective*, *U.S. Geol. Survey Professional Paper* (Vol. 1360, pp. 25–42).

Zoback, M., Zoback, M. L., Mount, V., Suppe, J., Eaton, J. P., Healy, J. H., et al. (1987). New evidence on the state of stress of the San Andreas fault system. *Science*, *238*(4830), 1105–1111. https://doi.org/10.1126/science.238.4830.1105